Not cutting corners: Bioderived triggers driving oxidative main chain scission of Polyethylene terephthalate

Dhananjay Dileep,[†] Michael J. Forrester,[†] Jack Bonde,[†] Valentina Camelo Vega,[†] Lauren Burton,[†] Ting-Han Lee,[†] Aleksei Ananin,[†] Baker Kuehl,[†] George A. Kraus,[‡] and Eric W. Cochran[*,†]

†*Department of Chemical & Biological Engineering, Iowa State University, Ames, Iowa 50011, United States*

‡*Department of Chemistry, Iowa State University, Ames, Iowa 50011, United States*

E-mail: ecochran@iastate.edu

Abstract

About 20-34 billion polyethylene terephthalate (PET) bottles from the beverage industry leak into aquatic ecosystems annually, necessitating the development of urgent strategies to treat waterborne plastic pollution. Inspired by the scalability of water disinfection infrastructure and protocols, we present a dual depolymerization approach relying on oxidation followed by hydrolysis. Incorporating bio-derived monounsaturated C18 diacid (C18:1-DA) counits at low dosages (2-5%) in the PET backbone overcomes the diffusional limitations of depolymerizing PET in the solid state by suppressing the glass transition temperature of the copolymer by 20°C. Cryomilled C18:1-PET powder suspended in an oxidant-loaded alkaline slurry underwent bulk depolymerization to oligomers at 80-100°C via oxidative scissions at the

internally located unsaturations. In contrast, conventional PET only undergoes minor end-chain scission in mild alkaline conditions. These oligomers are suitable for low-energy repolymerization or facile solvolysis to monomers. A permanganate-periodate oxidant couple demonstrates successful oxidation through the bulk of the polymer, which subsequently was hydrolyzed to monomers. This model system serves as a proxy for ozonolysis followed by mild hydrolysis to reduce the energetics of alkaline hydrolysis. This integrated oxidation-hydrolysis strategy paves the way for the industrial adoption of cleaner, advanced oxidation processes such as ozonolysis for plastic pretreatment, further enabling commercialized chemical recycling of unsaturation-containing polyesters.

Keywords

PET, chemical recycling, ozonolysis, oxidation, depolymerization

Introduction

Polyethylene terephthalate (PET) took the packaging realm by storm, swaying consumer choice swiftly from buying beverages packaged in glass or aluminum to using a lightweight, transparent, durable, and inexpensive alternative. The market share nearly tripled as PepsiCo and Coca-Cola diversified in the Reverse Osmosis (R.O.) industry.[1] Ever since, it has prevailed as a manufacturer and consumer's favorite, offering an optimal balance of thermomechanical properties, optical clarity, chemical resilience, and impermeability to moisture, oxygen, and carbon dioxide.[2,3] However, a global production rate of about 40 Million Metric Tons (MMT)[4,5] of non-biodegradable PET waste imposes an immense environmental burden, occupying 12 vol % of all Solid Waste (S.W.).[6] Additionally, PET recycling rates have dipped by 2.3% since 2018 due to the COVID-19 pandemic as a knee-jerk response to the inflated demand for sanitary single-use disposable packaging options. The simultaneous closure of curbside collection and recycling facilities[7,8] has amplified waste outflow to secondary and tertiary recycling markets, necessitating

more robust and circular PET recycling programs.

The plastic waste crisis led to consolidated efforts toward mechanical recycling and incineration for power generation. However, the push towards advanced materials like multi-layer packaging and heterogeneity at both macro and micro levels to optimize product performance has seriously impeded thermomechanical recycling efforts. Even a highly segregated and low contaminant-containing PET bottle stream is recycled at a meager rate of 30%. This low ceiling in mechanical recycling rates can be attributed to the inferior product quality post-recycling. Mechanical recycling, albeit cost-effective and scalable, reprocesses PET at melt and high shear oxidation-prone conditions that promote random and β-chain scission events, drastically reducing molecular weight and melt viscosity or causing crosslinking, ultimately deteriorating the performance characteristics of the polymer.[9–13] Further, such resins accumulate contaminants, including heavy metals that cause discoloration and pose toxicity hazards. This behooves the engineering community to look for better recycling strategies that maintain engineering performance over multiple recycling lives of the product.

The shortcomings of mechanical recycling have prompted research efforts to keep carbon usefully sequestered in the ecosystem, thus looking at cradle-to-cradle chemical recycling methods. Various solvents can break down polyesters into conventional or value-added monomers using alcohols, amines, and water.[14–16] Though a perfect process conceptually, chemical recycling has not bloomed at economies of scale because of the high energetic demands,[17–19] expensive catalysts, or difficulty in separating the end products. Thus, there is a critical need to design innovative and sustainable pathways to chemically depolymerizing PET.

The study looks at a novel approach: redesigning the PET backbone with an oxidation-prone monounsaturated C18 diacid (C18:1) as a partial drop-in replacement of terephthalic acid. Analogous to the dihydroxy terephthalate Trojan Horse unit (T.H.) described by Lee et al., C18:1 is readily obtainable from the self-metathesis of inexpensive and

renewable oleic acid.[20] The inspiration to leverage the reactivity of internal unsaturation for initiating depolymerization stems from the commercialized process of ozonizing oleic acid into azelaic acid and pelargonic acid.[21,22] The unsaturation in the polymer backbone provides the locus for oxidative scission in the solid state, overcoming the high activation barrier of initiating hydrolysis at mild conditions. Upon oxidative scission, the oligomers produced are around the critical molecular weight or lower ($\approx M_c$), below which the entanglement effects diminish, allowing faster diffusion. This oxidative-hydrolytic approach offers several advantages over existing catalyzed solvolyses:

Oxidation via ozonolytic pretreatment can now be carried out by ozone that is generated efficiently at 8-15 kWh/kg O_3.[23,24] Further ozone generation can be readily adapted to a decarbonized electric grid reliant on wind and solar power that can potentially alleviate GHG emissions by nearly 50%. The ozone is required to only break the T.H. units, cutting the requirement to a mere fraction of the PET being depolymerized. This pretreatment can improve traditional chemical or chemoenzymatic depolymerization methods that require high temperatures and, subsequently, higher energy (40-60 MJ/kg of PET).[25] This could also mitigate the energy demands of the existing state-of-the-art processes like the Volcat process, which requires reaction temperatures of 200°C.[26] Ozone can be generated in situ, eliminating the need for expensive phase transfer catalysts such as triethylamine and their associated handling and recovery costs. Ozonolysis significantly boosts the atom economy by minimizing waste generation and eliminates the use of heavy metals for depolymerization. When coupled with mild hydrolytic conditions, this process can evolve into a panacea for eliminating or mineralizing recalcitrant organic and inorganic pollutants like dyes, pigment, and pesticides that carry over with plastic in packaging industries. This article demonstrates a scaled-down version of a visionary commercialized ozonolysis process with a surrogate permanganate-periodate oxidation couple. The final oxidation products of ozonolysis or permanganate-periodate are expected to be concordant.[27,28]

With the advent of clean, advanced oxidation protocols at economies of scale, we envision a process in the near future where plastic debris suspended in large water tanks is bubbled with ozone or other suitable oxidants, depolymerizing it into oligomers that can be repolymerized or can undergo facile hydrolysis. Recently, Liu et al. proved that PET oligomers obtained from chemical recycling can be digested by microorganisms that synthesize polyhydroxy alkanoates PHAs, underscoring the potential to upcycle low-energy depolymerization products biologically.[29] Quartinello et al.[30] demonstrated the feasibility of hydrolyzing PET oligomers using a chemoenzymatic approach utilizing *Humicola insolens* cutinase resulting in 97% pure TPA.

Results and Discussion

Stochastic incorporation of C18:1

High purity (>98%) of C18:1-DA with minimal oleic acid was obtained upon recrystallization to produce high molecular weight copolymers (see **Fig. 1** in the main text and **Fig. S1**-**Fig. S2** in the S.I.). Finally, a series of copolymeric C18:1-PET formulations were prepared by changing the C18:1 dosage during pre-polymerisation followed by polycondensation (**Fig. 1**), and their properties are summarised in **Tab. 1**.

^{1}H-NMR (cf. **Fig. S3**) corroborated the presence of the C18:1-DA counits in the backbone, as evidenced by the sp^2 carbon visible at 5.36 ppm. A slight discrepancy in C18:1 content between theoretical and actual C18:1 content (determined by NMR, **Tab. 1**) occurs due to a high-vacuum and high-temperature polycondensation that stripped the more volatile C18:1 diester from Bis (2-Hydroxyethyl) terephthalate (BHET). Gel permeation chromatography revealed that the synthesized series' relative molecular weight and dispersity (Đ) were comparable to lab-grade PET. This proved that the unsaturation did not participate in side reactions during polycondensation, which may result in branching. The T.H. modified polymers were then assessed for the distribution of these units across varying chain lengths.

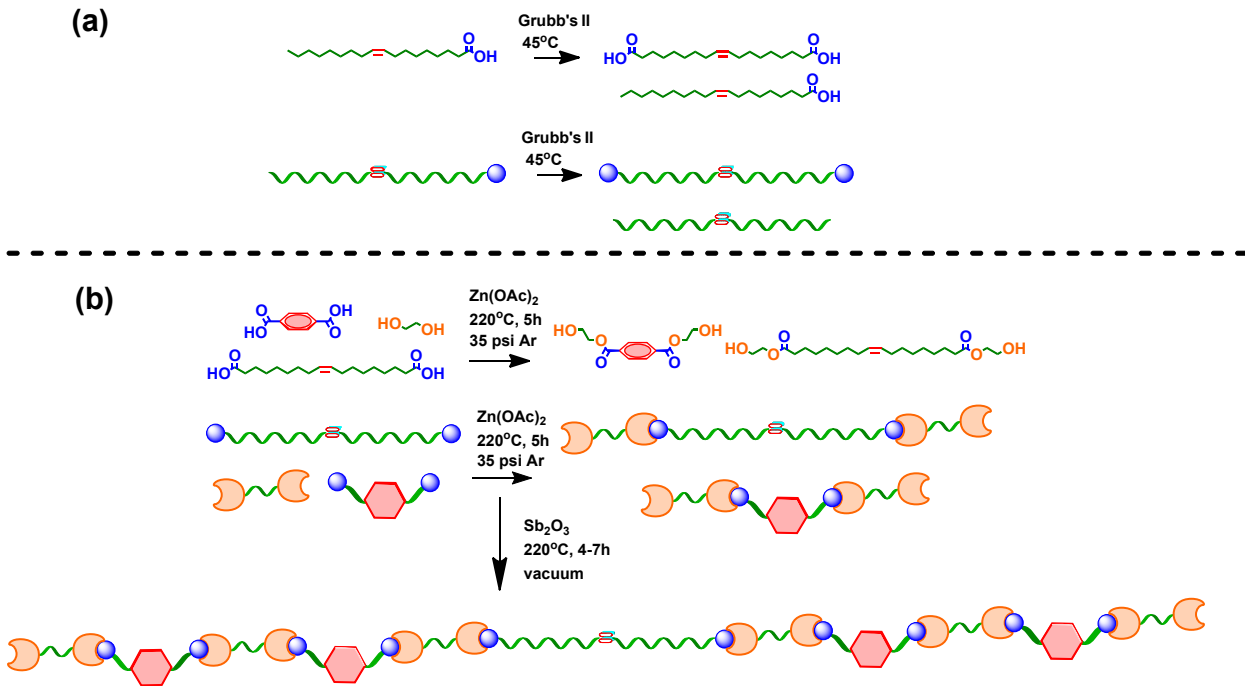

Figure 1 (a) C18:1-DA counit synthesis through self metathesis of Oleic Acid. (b) Synthesis of C18:1-PET-copolymers by substituting C18:1-DA as a drop-in replacement of Terephthalic Acid.

A retrosynthetic approach that oxidatively cleaved the double bond using ozone helped deduce the average loci of the C18:1 units across the polymer chains, illustrated in **Fig. 2a,b,c**. Selective ozonolytic cuts on a C18:1-PET sample solubilized in trifluoroacetic acid and chloroform left-shifted the mean molecular weight of the distribution commensurate with the % T.H. units in the chain (as predicted by NMR). For the C18:1-2.5% formulation (actual incorporation 2% by NMR red bar in **Fig. 2**a,b, ozonolysis reduces the M_n by nearly 50%, indicating that the C18:1 counits, on average, are centrally located across chains of varying lengths. Theoretically, these chain breaks can be present anywhere in the chain; however, initial co-esterification with excess TPA (terephthalic acid) masks the reactivity of C18:1 units with BHET termini and favors equal growth in both dimensions during polycondensation. The 5% target formulation (actual incorporation 4%) seems to have two C18:1 equidistant counits present per chain on average as M_n post ozonolysis reduces by a factor of three. The weight reduction by a factor of 4 post ozonolysis for the 5.8% formulation (See **Tab. 1** for % incorporation by NMR) indi-

Table 1 Chemical and physical properties of synthesized and commercially available C18:1 PET-based copolymers

Property	Lab PET	C18:1-PET-2.5%	C18:1-PET-5%	C18:1-PET-7.5%	Units
Target	0	2.5	5	7.5	%
Actual C18:1[a]	0	2	2.9	5.8	%
M_n[b]	41.6	34.7	29	36.1	kDa
M_w[c]	77	74.3	63.3	87.7	kDa
T_g[d]	78.3	69.6	59.6	46.1	°C
T_m[e]	249.2	242.9	247.6	242.5	°C
$T_{ch}^{on} - T_{ch}^{p}$[e]	20.9	13.1	18.4	20.0	°C
ΔH_m[f]	40.4	43.7	38.5	36.9	J/g
$\%X_{WAXS}$[g]	29	31	21	25	%
$2\theta^{\circ}$[h]	22.5	22.29	22.17	22.24	° (Deg)
E[i]	2.48±0.38	2.19±0.03	2.34±0.07	2.69±0.89	GPa
ε[j]	409.3±59.8	352.2±56.5	354.5±44.8	95.6±15.5	MPa
Tensile Strength	45.5±6.5	54.6±7.7	39.6±6.2	44.4±4.1	%

[a] D.U. represents the degree of unsaturation from C18:1 monomer, [b] Number-averaged molecular weight, [c] Weight-averaged molecular weight, [d] Melting transition temperature, [e] Difference in crystallization onset temperature and temperature of peak crystallization rate at 10 °C/min cooling (DSC),[f] Enthalpy of melting,[g] %Crystallinity from WAXS,[h] Centroid of the amorphous halo from WAXS [i]Young's Modulus, [j]Strain % (mm/mm)

cates that, on average, the 3 T.H. units were present equidistant across the distribution of chain lengths in the polymer. For the higher target dosages, random incorporation favors some non-equidistant loci for T.H. units, leading to less effective oxidative scissions.

The NMR plot in the **Fig. S4** corroborates the consumption of the unsaturation. This occurred without significantly distorting the shape of the molecular weight distribution, thus ruling out severe aggregation of C18 units and helping arrive at the modicum dosage of T.H. units that impart maximum recyclability without affecting thermomechanical or processing characteristics. Secondary evidence for their random incorporation can be inferred from a sustained decrease in melting point (as shown in **Tab. 1**) with increased non-crystallizable C18:1-unit dosage in the chain. Their optimal dosage and consequent scission thus will result in a molecular weight distribution of oligomers centered at or below a critical molecular weight ($M_{c,\,deploy}$), conceived to be critical to speeding up the depolymerization cascade.

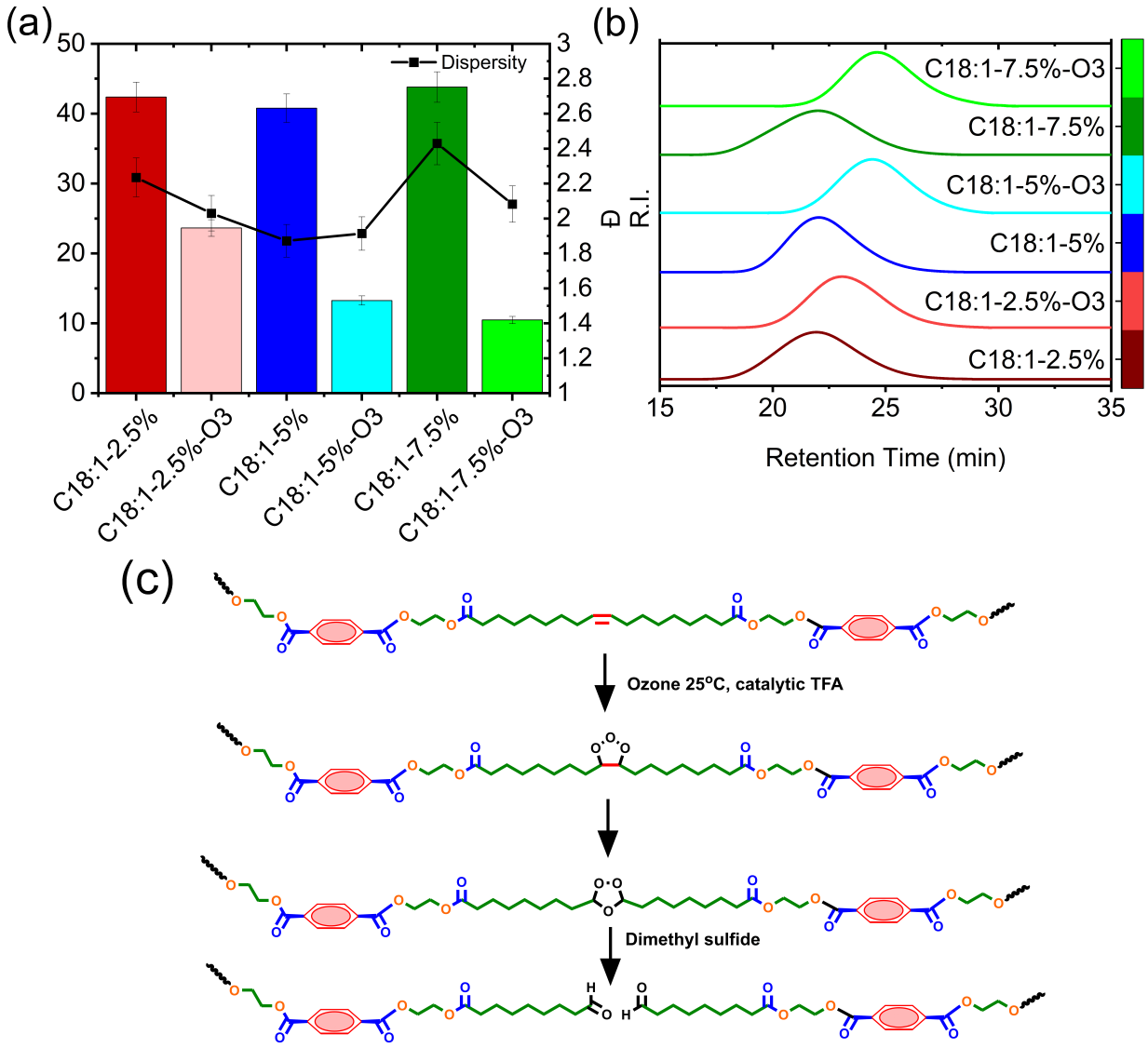

Figure 2 (**a**) Molecular weight reduction and tracking dispersity (Đ) of pre- and post-ozonolysis of C18:1-PET-copolymers. The darker color bars represent the pre–ozonolysis sample, and the lighter variants represent the same sample after the solution phase of ozonolysis. The reduction in molecular weight is commensurate with dosage, and the dispersity of the samples is denoted by the black line and, on average, stays around 2, indicating the cleavages occurred in almost all chains at the same location.(**b**) GPC chromatograms of pre and post-ozonolysis of C18:1-PET copolymers. Ozonolysis does not affect the peak dispersity significantly, and that shows that C18:1 units are present on almost equidistant internal locations across the chains of varying lengths. (**c**) Reaction mechanism illustrating reductive ozonolysis occurring at C18:1 sites embedded in the polymer leading to oxidative depolymerization

Thermomechanical and crystallization characteristics of the C18:1-PET copolymers:

C18:1 aliphatic spacers significantly altered the thermal behavior of the polymer (cf. **Fig. 3a,b** and **Tab. 1**). Increasing the flexible T.H. units in the chain significantly sup-

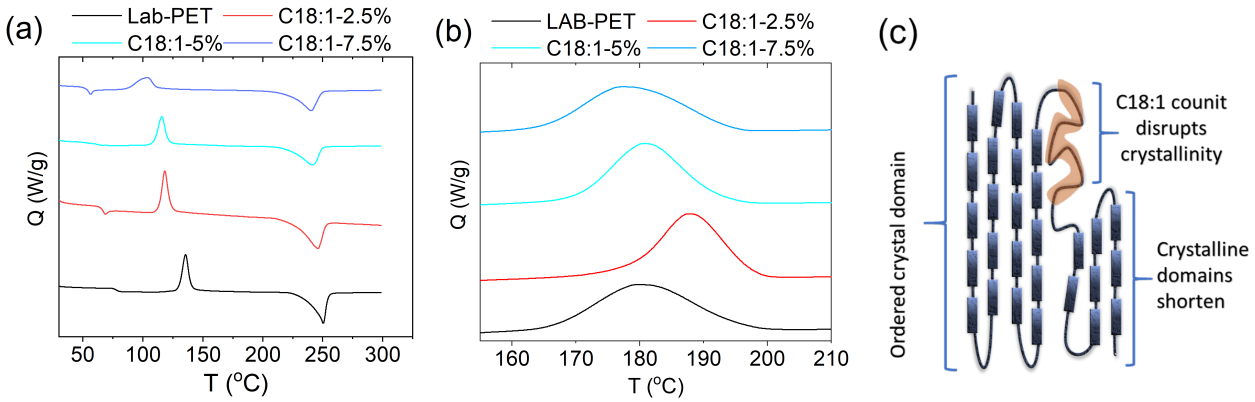

Figure 3 (**a**) DSC heating trace (2nd cycle) of C18:1-PET copolymers. This plot shows the T_g and T_m suppression shown by the C18:1-PET copolymers and a reduction in overall crystallinity shown by smaller and broader melt endotherms. (**b**) DSC cooling trace (1st cycle) of C18:1-PET copolymers illustrating recrystallization from the melt. The peak broadens as the dosing of C18:1 unit increases beyond 5% while sharpens for the 2.5% loading at the ramp rate of 10°C/min. (**c**) The disruptive effect of a T.H. unit on a crystal lamella may reduce overall crystallinity. A crystalline monomer may be envisaged that represents a unit cell within a lamella, which will likely get disrupted by the presence of a non-crystallizable T.H. unit. This is captured in the DSC for the 7.5% target formulation with suppressed T_g and T_m.

presses the T_g, indicating a lower energy barrier for committing long-chain motion. These formulations also reduced local ester density along the backbone while emerging as point defects along the lattice and suppressing the T_m of the copolymer. **Fig. 3**c illustrates the influence of a disruptive T.H. unit near a crystal lamella, hindering the formation of a crystal structure.

These structurally dissimilar and intrinsically flexible C18:1 comonomers alter the crystallization characteristics and kinetics of the system. At low incorporation ratios (2.5% mole incorporation), these counits suppress the T_g by 10 °C and provide heterogeneous nucleating sites, facilitating a faster onset of crystallization from the glassy state. This is also corroborated by the WAXS analysis carried out on annealed injection molded samples.% X (crystallinity) remains largely unchanged, most likely due to heterogeneous nucleation. Still, the centroid of the amorphous halo moves to a lower 2θ value (cf.**Tab. 1** and **Fig.** S5), indicating that average d-spacing between crystal lamella increases. This hints that the C18 units aggregate in the amorphous domains of the

copolymer, as no new crystalline peaks are observed. Above 5 mol % dosage, a faster onset of crystallization ensues because of a 30 °C drop in T_g at the expense of an overall reduction in crystallization (cf. **Tab. 1**) due to disruption in the conventional packing characteristics of a PET system. %X from WAXS was closer to thermally equilibrated crystallinity values as the dogbones were annealed for 24h at 150°C. On the other hand, modulated DSC (mDSC) provides a better kinetic appreciation of phase change phenomena since the PET and C18:1 copolymers samples are not in thermodynamic equilibrium at ramp rates of 10°C/min. The mDSC panel (**Fig.** S6 (a)-(d) decouples kinetic and thermodynamic components associated with melting. PET is known to undergo annealing before it recrystallizes to a thermodynamically stable polymorph.[31] Introducing C18:1 units in low dosage can severely affect the crystallization kinetics with minor changes in total crystallinity until higher dosages (5%) are introduced in the backbone. The red trace is the non-reversing component of the heat flow, which captures the dynamics of simultaneous recrystallization during melting, which is not clearly observable for a normal DSC. As the C18:1 component increases, T_g suppression favors the onset of early "silent crystallization" unobservable on the total signal. This explains that at minimal incorporation ratios, T_m suppression may not be resolved cleanly at fast linear ramp rates.

ΔH_m, and T_m only drop conspicuously (at $\geq$ 5% incorporation) with a consequent gain in the compositional and conformational entropy of flexible and rubbery C18:1-PET systems. The T.H. unit is expected to fractionate in the amorphous domains and get pushed out of the surface of the crystal upon phase equilibration. These will preclude the densification of spherulites; however, at low loadings, these can plasticize the system by acting as amorphous tie segments between two crystal domains and cause rapid kinetic perfection of PET polymorphs.

The trends are mirrored during recrystallization from the melt. A modicum of C18:1 units allows for rapid nucleation, faster onset, and overall growth of crystals, evidenced

by a sharp recrystallization peak. However, at 7.5% target loadings, a delayed onset of crystallization with a broad peak is observed, most likely due to the system adopting disruptive conformations for stable nuclei to grow.

An analogous trend is observed in the mechanical characterization as C18:1 copolymers undergo rapid necking and increased elongation before the break (cf. **Tab. 1** and **Fig.** S7). Flexible C18 units impart strain rate sensitivity to the elongation behavior. At slow strain rates (10 mm/min), the elongation characteristics of 2.5% formulation resemble conventional PET as the polymer is still in a vitreous state. The strain rate primarily governs the crystallization rate. A modicum of C18:1 content increased the crystallinity of the copolymers compared to their conventional counterparts upon stretching. This difference may broaden if the strain rate is increased 10-fold. However, the effect of these counits becomes prominent at loadings exceeding 5% as T_g is close to room temperature, resulting in a faster chain alignment than relaxation rates to random configurations despite a sluggish strain rate. Above 5% loadings, the rubbery amorphous segments expand while the mesophase precursor to strain-induced crystallization shrinks, resulting in premature failure ($\varepsilon \approx 95\%$, cf. **Tab. 1**) before significant elongation. The tensile strength reported in **Tab. 1** reflects the extent of strain-induced crystallization. Lower C18:1 content increased tensile strength, indicating higher crystallinity upon break, which may be a valuable property for light load-bearing applications. The T_g-$T_{stretch}$ along becomes exceedingly important in determining % crystallinity as a function of time during tensile strength tests.

Oxidative scission of T.H. units with permanganate-periodate couple:

The C18:1 PET copolymers can be oxidatively cleaved with potassium permanganate-sodium metaperiodate under prolonged heating to carboxylic acids. It is critical to increase the half-life of the permanganate oxidant to the time scales (several days for very dilute alkaline systems) required for diffusion-limited slurry reactions. Upon oxidative

scissions, the resulting low molecular weight oligomers could then be solvolyzed under mild conditions.

The permanganate-periodate couple oxidizes C18:1-PET slurries at temperatures 80, 90, and 100°C. The unsaturation undergoes oxidative addition of the permanganate ion, forming a cyclic hypomanganate Mn^{5+} diester, which hydrolyses to a cis diol.[32] The metaperiodate cleaves the cis-diol to a diacid. Mn^{5+} could disproportionate to the Mn^{4+} and Mn^{6+} states; however, under alkaline oxidative conditions, the hypomanganate is likely to rearrange to a manganate Mn^{6+} state exclusively, delaying the formation of a less powerful but thermodynamically stable insoluble oxidant MnO_2. Periodate rapidly funnels Mn^{6+} towards the Mn^{7+} state, as typically, the rates of periodate oxidation greatly exceed the rate of disproportionation of Mn^{5+}.[33] This cascade results in continuous permanganate regeneration for a prolonged interval by periodate. The plausible mechanism is illustrated in **Fig. S8**. The Latimer diagram also suggests a higher reduction potential of 0.70 V in the alkaline medium for periodate going to iodate than manganate to permanganate, which is 0.56 V. This increases the half-life of the higher oxidation state species Mn^{7+}. As the reaction zone is limited to a few layers below the surface and expands with the denudation of the polymer particles, the metaperiodate co-oxidant maintains the longevity of Mn^{7+} on both bulk and fresh surfaces, minimizing the amount of permanganate required for the solution.

The alkaline medium promotes end chain and random scission; however, these events occur primarily at the surface as PET is not easily wetted. The hydrolysis eventually releases ethylene glycol and oligomers, which may act as phase transfer catalysts for permanganate to reach the bulk of the polymer. Also, hydrophilicity increases steadily with both oxidative and hydrolytic operative modes of scission, increasing the number of carboxylic chain ends. The oxidation dominant regime brings about coerced backbone scission at the T.H. units, resulting in oligomers that undergo quick and mild hydrolysis. T_g is chosen as a relevant temperature boundary to ensure that the depolymerization

occurs in the rubbery state of the semicrystalline polymer, mitigating the diffusional barriers in a heterogeneous reaction system.

NMR and GPC track the molar degree of unsaturation (% DU) and extent of depolymerization as a function of time. % DU alone may not reveal the number of chains cleaved as oxidative cleavage is a multistep process initiating the loss of double bonds to form cis diols and then ultimately breaking down into diacids. **Fig. 4**a,b tracks the % DU in the residual partially reacted solids phase across the C18:1-PET copolymers in the relevant oxidation reaction space. Ejected monomers are entirely soluble in the alkaline medium. At 100°C, the control set comprising C18:1-PET in the absence of oxidant (**Fig. S9**) exhibited a slight reduction in molecular weight due to inconspicuous chain end hydrolysis occurring at the surface with no change in % DU **Fig. S9** also hints at bulk depolymerization as the aromatic region develops peak ramifications that are suspected to arise due to oligomers of different chain lengths).

GPC of the residual solid post-depolymerization discerns the dominant mode of depolymerization with time and the sensitivity of temperature of these reactions as a function of T.H. dosage, shown in **Fig. 4c,d**. C18:1-2.5% vs. C18:1-5% formulations respond differently to a 10 °C rise in reaction temperature, i.e., from 80 to 90°C. The differential arises from a T_g suppression of 7 °C for the 5% loading, and in effect, enhanced chain mobility grants access to the oxidant. **Fig. 4**c,d shows that this effect is pronounced at 80°C between the two formulations (i.e., 2.5% and 5%), marked by the exponential consumption of olefin by the oxidant for the 5% formulation as opposed to nearly linear slope for the 2.5% formulation. This difference in the rate of oxidant transport across the polymer chains wanes when the reaction temperature exceeds T_g by 15-20°C. We hypothesize that T_{rxn}-T_g is the critical determinant for qualitatively assessing the accessibility of olefinic moiety by the oxidant. The insolubility of the oligomers and the heterogeneous nature of the reaction with mixed salts obfuscate clear mass loss trends, which is why GPC is used to assess depolymerization.

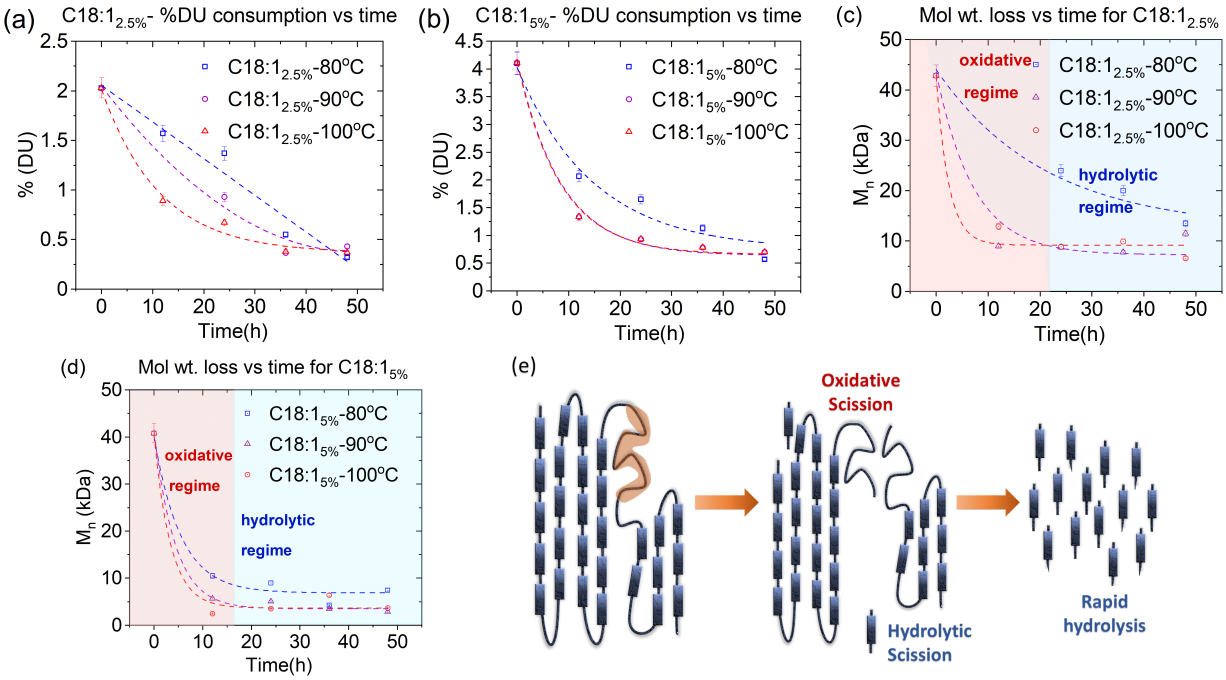

Figure 4 (a) % DU vs. time in C18:1-2.5%-PET system. This graph is generated by tracking double bond consumption by NMR. For a 2.5% formulation, rapid oxidation prevails at temperatures exceeding T_g by 20°C, achieved at 90°C. (**b**) % DU consumption in C18:1-5%-PET system. Rapid oxidation is achieved at 80°C as the T_g for a 5% formulation is further suppressed, resulting in easier oxidant transport in the rubbery state of the copolymer. (**c**) Oxidative hydrolysis of C18:1-PET for 2.5% formulation. The oxidative regime causes initial loss in molecular weight as the double bond gets consumed as the C18:1 unit occupies nearly equidistant internal locations on the chain. This rate of molecular weight loss falls as the oxidant-prone moiety gets consumed and results in easily hydrolyzed oligomers. The molecular weight loss mirrors the % D.U. consumption curve, illustrating the faster weight loss as reaction temperature exceeds T_g by $\approx$ 20°C. (**d**) Oxidative hydrolysis of C18:1-PET for 5% formulation. Steeper molecular weight loss happens due to oxidative cleavages that are more rampant in a 5% formulation vis-à-vis the 2.5% formulation. The lower T_g and more oxidant-prone moieties allow for faster onset of hydrolytic scissions. (**e**) Oxidant attack on the C18:1 unit and subsequent hydrolysis of the semicrystalline C18:1-PET copolymer. The disruptive C18:1 unit reduces the overall crystallinity and lends a site for easy oxidative scission in the rubbery state. The C18:1 unit may fractionate in the tie-strand region between two crystalline domains, which is cleaved off by the oxidant that unspools the crystalline domain and allows easier hydrolysis of the oligomers.

The oxidative scission proceeds through the bulk of the polymer, as evidenced by the multimodality of GPC traces of the residue. Multimodal peaks are deconvoluted and assigned, and a compositional average is computed for M_n that captures the rate at which the reaction progresses with effective cuts in the chain. The trends mirror the

% DU consumption, with T_{rxn}-T_g being the dominant factor in the oxidation rate. The M_n vs. T dependence mirrors the trend of % DU consumption. Molecular weight loss follows an Arrhenius decay with time for both formulations, as described in **Fig. 4**c,d and **Tab. S1**. The ceiling molecular weight of oligomers obtained after 48 hours shows 2× efficiency of oxidative cuts for the 5% vis-a-vis the 2.5%, corroborating tertiary evidence to the random distribution of C18 units in the chain.

The molecular weight decay follows an expression (shown in Eq. 1) of the form as follows:

$$M_n = A_1 \exp\left(-\frac{t}{\tau}\right) + M_t \tag{1}$$

Where A_1 is an Arrhenius prefactor, and the time constant τ is temperature dependent as oxidant access starkly increases with temperature while weakly influenced by hydrolysis due to the mild alkaline nature of the solution and surface depolymerization. The molecular weight approaches the critical length of the oligomer transient (M_t) post oxidation before it starts hydrolyzing extremely fast into monomers.

The τ term captures the temperature sensitivity of the oxidative hydrolysis. Most alkene is consumed within 48 hours, proving the oxidant's permeance inside the polymer's bulk. The same experiments at 100°C reveal an increased monomer ejection rate due to faster hydrolysis; however, the half-life of Mn^{7+} could be negatively impacted, favoring more Mn^{4+} in the medium that may slightly slow down oxidation.

The experimental conditions at 80°C, 90°C, and 100°C reveal the competing nature of both hydrolysis and oxidation, with the rate of oxidation being a function of temperature, with the most potent oxidant consumed more rapidly compared to the diffusional time scale resulting in overall slower oxidation. This hints at the optimum temperature between 90°C and 100°C prevailing at existing reaction concentrations. Also, a second optimum might be evident at higher temperatures, where a short burst of high temperature will allow faster hydrolysis, reduced dielectric constant, and faster breach of the oxidant to the olefinic moiety inside the chain. The overall molecular weight loss

trends indicate that the hydrolytic rate significantly increases after M_t at prevailing conditions. This is corroborated by increased monomer yield as intermediate oligomeric species ($M_{oligomer} < M_t$) are very short-lived. This combined oxidative and hydrolytic depolymerization pathway paves the way to leverage the intrinsic reactivity of T.H. units to help overcome the mass transport barriers of the semicrystalline PET system.

Conclusion

Unmodified PET is recalcitrant to facile chemical depolymerization. This study objectively demonstrates that a minor modification of PET with an inbuilt trigger-responsive site unlocks depolymerizability. Selective reactions, easily achievable on a small molecule scale, can be mirrored relatively quickly on the macromolecular scale. An aliphatic spacer that equilibrates in the amorphous domains is an accessible center to initiate depolymerization. Further bulk reaction ensures the crystalline domains crumble, decrepitating the polymer to rapid depolymerization. A slight perturbation of the polymer's structural fingerprint with an aliphatic segment might open the doors to advanced green and scalable oxidation protocols. This proxy permanganate-periodate reaction is a model for (pre-)commercial oxidation processes such as ozonolysis that can be used with mild hydrolysis for T.H. laced polymer systems, significantly bringing down the energetics of solvolysis.

Conflicts of Interest

No interests to declare.

Supporting Information Available

Supplementary information comprises the experimental details, including methods and materials used. It also has additional NMR spectra of C18-copolymer pre and post oxi-

dation, results from modulated DSC and WAXS for determining crystallinity and tensile data for specimens.

Acknowledgement

This material is based upon work supported by the U.S. Department of Energy's Office of Energy Efficiency and Renewable Energy (EERE) under the Bioenergy Technologies Office Award number DE EE0009294. The views expressed herein do not necessarily represent the views of the U.S. Department of Energy or the U.S. Government.

Notes and references

1. Parker, L. How the plastic bottle went from miracle container to hated garbage. 2019; `https://www.nationalgeographic.com/environment/article/plastic-pollution`, Accessed: 2024-11-07.

2. Bartolome, L.; Imran, M.; Cho, B. G.; Al-Masry, W. A.; Kim, D. H. Recent developments in the chemical recycling of PET. *Material recycling-trends and perspectives* **2012**, *406*, 576–596.

3. Thomas, S.; Rane, A. V.; Kanny, K.; Abitha, V.; Thomas, M. G. *Recycling of polyethylene terephthalate bottles*; William Andrew, 2018.

4. Rorrer, N. A.; Nicholson, S.; Carpenter, A.; Biddy, M. J.; Grundl, N. J.; Beckham, G. T. Combining reclaimed PET with bio-based monomers enables plastics upcycling. *Joule* **2019**, *3*, 1006–1027.

5. Geyer, R.; Jambeck, J. R.; Law, K. L. Production, use, and fate of all plastics ever made. *Science advances* **2017**, *3*, e1700782.

6. Benyathiar, P.; Kumar, P.; Carpenter, G.; Brace, J.; Mishra, D. K. Polyethylene terephthalate (PET) bottle-to-bottle recycling for the beverage industry: a review. *Polymers* **2022**, *14*, 2366.

7. Goldsberry, C. US PET Bottle Recycling Rate Dips in 2019, According to NAPCOR Report. 2020; https://www.plasticstoday.com/packaging/us-pet-bottle-recycling-rate-dips-in-2019-according-to-napcor-report, Accessed: 2024-11-07.

8. Staub, C. US PET Bottle Recycling Rate Continues to Sink. 2021; https://resource-recycling.com/plastics/2021/11/03/us-pet-bottle-recycling-rate-continues-to-sink/, Accessed: 2024-11-07.

9. Oblak, P.; Gonzalez-Gutierrez, J.; Zupanc ic , B.; Aulova, A.; Emri, I. Processability and mechanical properties of extensively recycled high density polyethylene. *Polymer Degradation and stability* **2015**, *114*, 133–145.

10. La Mantia, F. P.; Vinci, M. Recycling poly (ethyleneterephthalate). *Polymer Degradation and Stability* **1994**, *45*, 121–125.

11. Deng, J.; Li, K.; Harkin-Jones, E.; Price, M.; Karnachi, N.; Kelly, A.; Vera-Sorroche, J.; Coates, P.; Brown, E.; Fei, M. Energy monitoring and quality control of a single screw extruder. *Applied Energy* **2014**, *113*, 1775–1785.

12. Gryn'ova, G.; Hodgson, J. L.; Coote, M. L. Revising the mechanism of polymer autooxidation. *Organic & biomolecular chemistry* **2011**, *9*, 480–490.

13. Schyns, Z. O.; Shaver, M. P. Mechanical recycling of packaging plastics: A review. *Macromolecular rapid communications* **2021**, *42*, 2000415.

14. Hong, M.; Chen, E. Y.-X. Chemically recyclable polymers: a circular economy approach to sustainability. *Green Chemistry* **2017**, *19*, 3692–3706.

15. Fukushima, K.; Lecuyer, J. M.; Wei, D. S.; Horn, H. W.; Jones, G. O.; Al-Megren, H. A.; Alabdulrahman, A. M.; Alsewailem, F. D.; McNeil, M. A.; Rice, J. E.; others Advanced chemical recycling of poly (ethylene terephthalate) through organocatalytic aminolysis. *Polymer Chemistry* **2013**, *4*, 1610–1616.

16. Carta, D.; Cao, G.; D'Angeli, C. Chemical recycling of poly (ethylene terephthalate)(PET) by hydrolysis and glycolysis. *Environmental Science and Pollution Research* **2003**, *10*, 390–394.

17. Ragaert, K.; Delva, L.; Van Geem, K. Mechanical and chemical recycling of solid plastic waste. *Waste management* **2017**, *69*, 24–58.

18. Elsaeed, S. M.; Farag, R. K. Synthesis and characterization of unsaturated polyesters based on the aminolysis of poly (ethylene terephthalate). *Journal of applied polymer science* **2009**, *112*, 3327–3336.

19. Pudack, C.; Stepanski, M.; Fässler, P. PET Recycling–Contributions of crystallization to sustainability. *Chemie Ingenieur Technik* **2020**, *92*, 452–458.

20. Lee, T.-H.; Forrester, M.; Wang, T.-p.; Shen, L.; Liu, H.; Dileep, D.; Kuehl, B.; Li, W.; Kraus, G.; Cochran, E. Dihydroxyterephthalate—a trojan horse PET counit for facile chemical recycling. *Advanced Materials* **2023**, *35*, 2210154.

21. McCoy, M. Making ozonolysis safe for manufacturing. *C&EN Global Enterprise* **2017**, *95*, 38.

22. Yan, K.; Wang, J.; Wang, Z.; Yuan, L. Bio-based monomers for amide-containing sustainable polymers. *Chemical Communications* **2023**, *59*, 382–400.

23. Katsoyiannis, I. A.; Canonica, S.; von Gunten, U. Efficiency and energy requirements for the transformation of organic micropollutants by ozone, O3/H2O2 and UV/H2O2. *Water research* **2011**, *45*, 3811–3822.

24. Ried, A.; Mielcke, J.; Wieland, A. The potential use of ozone in municipal wastewater. *Ozone: Science & Engineering* **2009**, *31*, 415–421.

25. Gracida-Alvarez, U. R.; Xu, H.; Benavides, P. T.; Wang, M.; Hawkins, T. R. Circular economy sustainability analysis framework for plastics: application for poly (ethylene terephthalate)(PET). *ACS Sustainable Chemistry & Engineering* **2023**, *11*, 514–524.

26. Allen, R. D.; James, M. I. *Circular Economy of Polymers: Topics in Recycling Technologies*; ACS Publications, 2021; pp 61–80.

27. Garti, N.; Avni, E. The oxidation of oleic acid by permanganate in oil in water emulsion. *Colloids and Surfaces* **1982**, *4*, 33–41.

28. Sam, D. J.; Simmons, H. E. Crown polyether chemistry. Potassium permanganate oxidations in benzene. *Journal of the American Chemical Society* **1972**, *94*, 4024–4025.

29. Liu, P.; Zheng, Y.; Yuan, Y.; Han, Y.; Su, T.; Qi, Q. Upcycling of PET oligomers from chemical recycling processes to PHA by microbial co-cultivation. *Waste Management* **2023**, *172*, 51–59.

30. Quartinello, F.; Vajnhandl, S.; Volmajer Valh, J.; Farmer, T. J.; Vonc ina, B.; Lobnik, A.; Herrero Acero, E.; Pellis, A.; Guebitz, G. M. Synergistic chemo-enzymatic hydrolysis of poly (ethylene terephthalate) from textile waste. *Microbial biotechnology* **2017**, *10*, 1376–1383.

31. Hiramatsu, N.; Hirakawa, S. Melting behavior of poly (ethylene terephthalate) crystallized and annealed under elevated pressure. *Polymer Journal* **1980**, *12*, 105–111.

32. Lee, D. G. *The Oxidation of Organic Compounds by Permanganate Ion and Hexavalent Chromium*; Open Court, 1980.

33. Lister, M.; Yoshino, Y. The oxidation of manganate by periodate. *Canadian Journal of Chemistry* **1960**, *38*, 2342–2348.

Nontechnical synopsis

This article establishes a synthetic pathway to render PET amenable to selective and mild chemical recycling, enabling a sustainable circular economy.

Supporting Information:

Not cutting corners: Bioderived triggers driving oxidative main chain scission of Polyethylene terephthalate

Dhananjay Dileep,[†] Michael J. Forrester,[†] Jack Bonde,[†] Valentina Camelo Vega,[†] Lauren Burton,[†] Ting-Han Lee,[†] Aleksei Ananin,[†] Baker Kuehl,[†] George A. Kraus,[‡] and Eric W. Cochran[*,†]

†*Department of Chemical & Biological Engineering, Iowa State University, Ames, Iowa 50011, United States*

‡*Department of Chemistry, Iowa State University, Ames, Iowa 50011, United States*

E-mail: ecochran@iastate.edu

List of Figures

List of Tables

Supporting Information

Experimental Details

Synthesis of C18:1-Diacid: 28.2g oleic acid (0.1 mol) (90% purity, technical grade) was charged in a reactor vessel with argon sparge maintained at 45°C for 30 minutes. 12.7 milligrams (15µmol) of Grubbs 2nd generation catalyst was wetted with 10 mL of hexane, purged with argon, and pressure fed into the reactor maintained at 45°C for 24 hours. The precipitate (diacid) was washed with hexane and recrystallized with ethyl acetate-hexane mixtures and toluene 3-5 times until product purity of ≈99% was achieved.

Prepolymer synthesis: The required number of precursors: (Z)-octadec-9-enedioic acid, terephthalic acid (molar ratios C18:1/TPA ranging from 2.5-7.5%), 0.1% zinc acetate and 6.5-10 eq excess ethylene glycol (EG) were transferred to a 300 mL stainless steel Parr reactor equipped with a paddle agitator, thermocouple, and dip tube. Temperature and pressure were maintained at 220°C and 110 psi, respectively, with a mild argon sparge maintained over the reaction mass for 5 hours to remove water and drive reaction equilibrium. The product was distilled under a vacuum for 2-3 hours at 125 °C to remove excess ethylene glycol from the mixture.

Polycondensation: Prepolymers BHET and C18:1 glycol adducts undergo polycondensation with catalytic (0.02 mole%) antimony trioxide at a temperature of 240-260 under about 23 psi dynamic vacuum (See Fig. A1 in Appendix). Intense agitation (250 RPM) and high vacuum ensured rapid removal of EG The reaction lasted 5-7 hours to achieve a high molecular weight. The melt was rapidly quenched upon contact with air and cryomilled. The fine powder is vacuum-dried to reduce the moisture content of the particles and to prevent agglomeration during prolonged storage. Relative molecular weight was determined by Gel Permeation Chromatography (GPC) against polymethylmethacrylate (PMMA) standards. NMR tests were performed to check for unsaturated functionalization of PET.

Oxidative cleavage of the copolymer using $KMnO_4$-$NaIO_4$ couple: 1g of C18:1-PET was added to a 30 ml solution of 0.036M KOH solution with 0.055mol $KMnO_4$ and 0.0028mol $NaIO_4$ and heated to 35°C while stirring for dissolution of $KMnO_4$. The reaction was conducted at 80, 90 and 100°C for 12-48 h. Upon reaction completion, the slurry was filtered. The residue was acidified with the slow addition of HCl accompanied by the exothermic bubbling at 64°C until the residue contaminated with MnO_2 turned faint yellow to nearly colorless, indicating the endpoint for reduction of Mn^{7+}/Mn^{4+} ions to Mn2+ ions. The slurry was filtered, and the residue was washed with water and vacuum-dried. Finally, the residue was characterized to quantify the extent of depoly-

merization. The process is repeated for different incorporation ratios of the C18:1-diacid in the copolymer.

Ozonolysis: The finely divided polymer obtained after cryo-milling was solubilized in trifluoroacetic acid. The reaction contents were vigorously stirred to reduce external diffusional resistance with ozone bubbling at a rate of 0.4 mmol/min for 30 minutes using an ozone generator (Ozonology Model L-100). The temperature was maintained well below 25°C using a water bath. This was followed by adding 0.1ml of DMS (dimethyl sulfide) while the reaction slowly equilibrated to room temperature. Aliquots were taken, and the reaction was quenched by precipitating the polymer upon adding water as a nonsolvent. The polymer was filtered, vacuum dried to the strip residual solvent, and characterized by GPC and NMR to quantify the extent of depolymerization and alkene consumption.

NMR Spectroscopy: 1H NMR spectroscopy (Avance III 600MHz) was performed on precursors, neat C18:1-PET copolymers, and oxidized samples using $CDCl_3$ and trifluoroacetic acid as a cosolvent. The raw spectral data was auto-phase and auto-baseline corrected using Bruker Topspin version 3.6. Spectral data were processed using M-Nova-14. Of primary interest is the C18:1 composition both as-synthesized and throughout depolymerization; the degree of unsaturation (%DU) is thus defined as follows:

$$\begin{aligned}\%\text{DU} &= \frac{\text{mol alkene}}{\text{mol alkene} + \text{mol terephthalate}} \times 100\% \\ &= \frac{\int \delta 5.35\,(2H, m)}{\int \delta 5.35\,(2H, m) + 2\int \delta 7.83\,(4H, s)} \times 100\%\end{aligned}$$

Differential scanning calorimetry (DSC): Differential scanning calorimetry was performed on (DSC, TA instruments Discovery 2500) to conduct a thermal analysis of the copolymer. Nitrogen was used as a purge gas at 50 ml/min. Samples were weighed and sealed in hermetically sealed aluminum pans. Each cycle consisted of heating the sample from 25°C to 300°C (ramp rate 10°C/min), isothermal equilibration for 5 minutes,

followed by cooling the sample back to 25°C (ramp rate 10°C/min). Two cycles were performed for each dataset. The T_g, H_f, and Thcon were computed for unoxidized samples.

Modulated Differential scanning calorimetry (mDSC): Modulated Differential scanning calorimetry was performed on (DSC, TA instruments Discovery 2500) to decouple kinetic and thermodynamic characteristics of melting. Nitrogen was used as a purge gas at 50 ml/min. Samples were weighed and sealed in hermetically sealed aluminum pans. Firstly, samples are equilibrated at 280°C (to erase thermal history) for 5 minutes and rapidly quenched at a cooling rate of 150°C to 0°C. Then, the sample is equilibrated to 25°C and heated at an average of 2°C/min with a sinusoidal temperature modulation amplitude of 0.318°C with a time period of 60 s to 280°C.

Gel Permeation Chromatography (GPC): Gel permeation chromatograms were recorded on Tosoh EcoSEC HLC-8320GPC, equipped with a U.V. and R.I. detector in tandem. Samples were pre-dissolved in trifluoroacetic acid (sample conc. $\approx$3 mg/ml), and 1,1,1,3,3,3-hexafluoroisopropanol (HFIP) was chosen as an eluent for PET-copolymers at a flow rate of 0.3ml/min. Samples were compared against PMMA calibration standards to determine M_n and M_w.

Tensile Testing: The various C18:1 PET formulations were dried under a high vacuum to remove moisture and injection molded into ASTM type 5-B dogbones using MiniLab/minijet at a mold temperature 25°C below T_g while maintaining the injection at 25°C above melting temperature to obtain mostly amorphous quenched samples. These were dried to remove any moisture picked up during storage, and a tensile strength test was performed at 10 mm/min for mechanical characterization of the sample. Four to five replicates per sample were tested. The Young's Modulus is computed with the help of an ARES G2 rheometer as there is slight sample slippage due to the relatively large grips of the UTM machine.

Wide Angle Xray Scattering Spectroscopy (WAXS): The crystal spacing and degree of crystallinity of injection molded C18:1 PET copolymers post 24 h of annealing at 150°C/min were investigated using a Xenocs Xeuss 2.0 Small- and Wide-Angle X-ray Scattering (S/WAXS) system with a Cu Kα X-ray source (λ = 1.542 Å). Scattered X-rays were collected using a Dectris Pilatus3 R 1M detector calibrated with a silver behenate standard. Samples were mounted directly onto the sample stage and measured under vacuum. WAXS data were acquired for 600s. Background scattering was measured under identical conditions for each sample.

Raw 2D scattering data were reduced and corrected for absolute intensity using Foxtrot 3.3.4 (SOLEIL Synchrotron, France). Subsequently, scattering profiles were combined using the Irena package (Advanced Photon Source, Argonne National Lab, USA).

Crystal structure information was extracted from the scattering vector (q) using the following equations:

$$q = \frac{4\pi \sin\theta}{\lambda} \tag{2}$$

$$d = \frac{2\pi}{q_{max}} \tag{3}$$

where θ represents Bragg's angle and q_{max} is the peak position in the q range.

The degree of crystallinity (X_c) was determined using the ratio of the crystalline fraction (A_c) to the total area ($A_a + A_c$) under the WAXS curve, as expressed by Scherrer equation (see Eq 4): An amorphous halo was generated by spline interpolation, and the centroid was calculated for each formulation, resolving information about the lamellar spacing as a function of copolymer dosage.

$$X_c = \frac{A_c}{A_a + A_c} \tag{4}$$

Additional Data

Table S1 Arrhenius Decay Parameters of Molecular Weight (M_t), Lifetime (τ), and Pre-Exponential Factor (A_1) in Oxidative Hydrolysis of C18:1-PET Systems

Sample	80°C	90°C	100°C
	C18:1-2.5%		
M_t (Da)	12393.9	9185.3	7257.3
τ (s)	20.9	2.4	7.2
A_1 (Da)	31674.7	33641.9	36296.3
	C18:1-5%		
M_t (Da)	6881.1	3490.7	3651.0
τ (s)	5.4	4.3	3.38
A_1 (Da)	33324.7	37904.8	37068.3

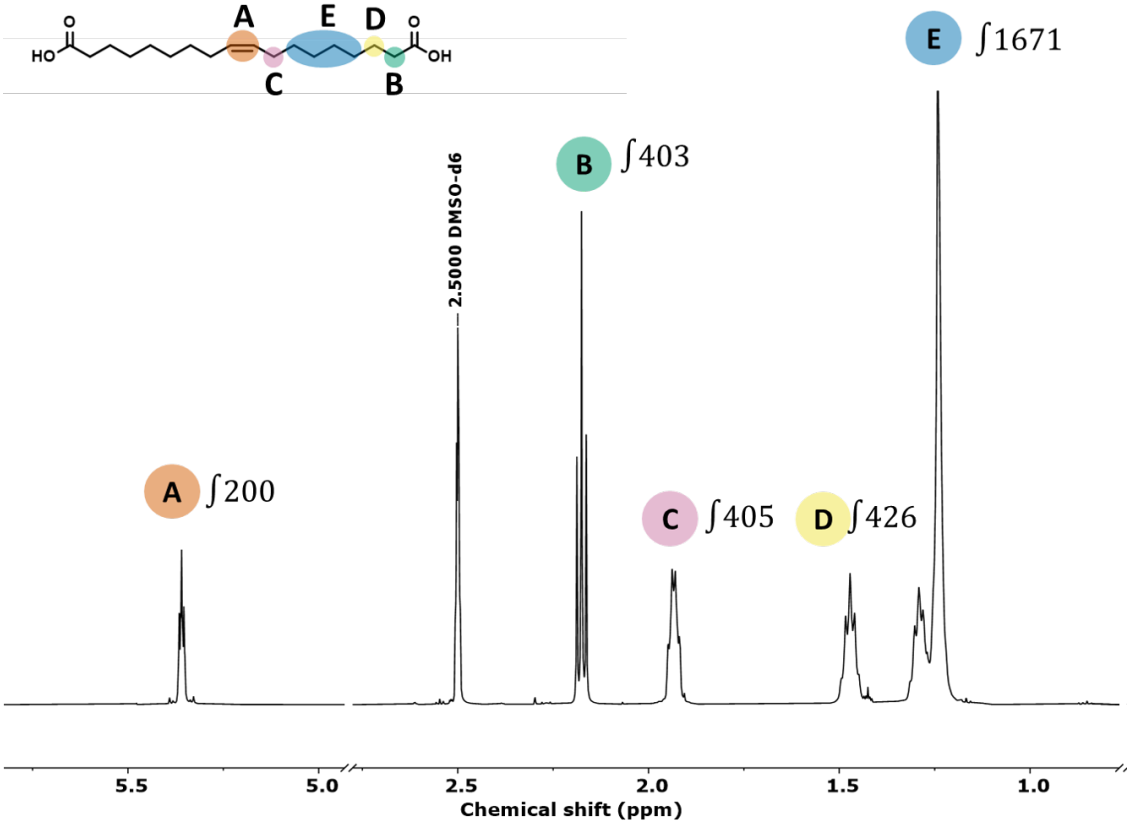

Figure S1 NMR spectra of C18:1 Diacid. This is prepared from the metathesis of oleic acid and recrystallized using ethyl acetate and hexane to remove the C18:1 alkene and unreacted oleic acid.

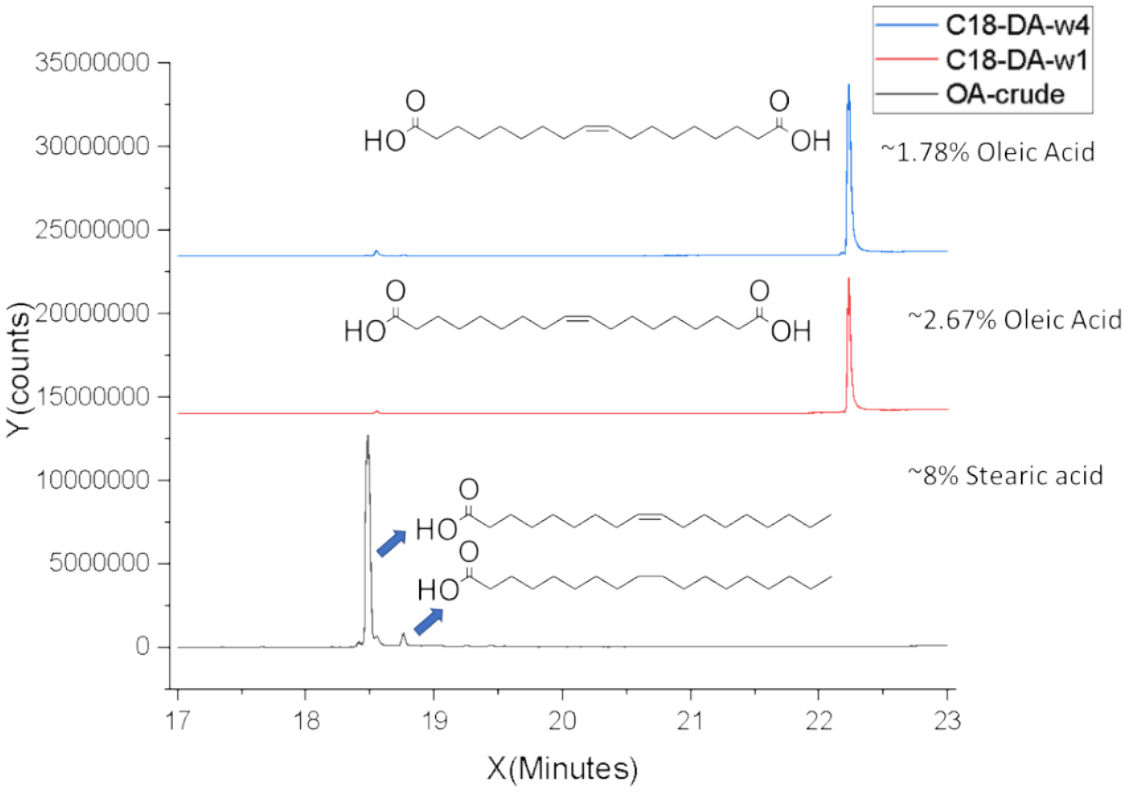

Figure S2 GCMS plot of purified C18:1 Diacid. Successive recrystallizations in ethyl acetate and hexane remove unreacted oleic acid (OA).

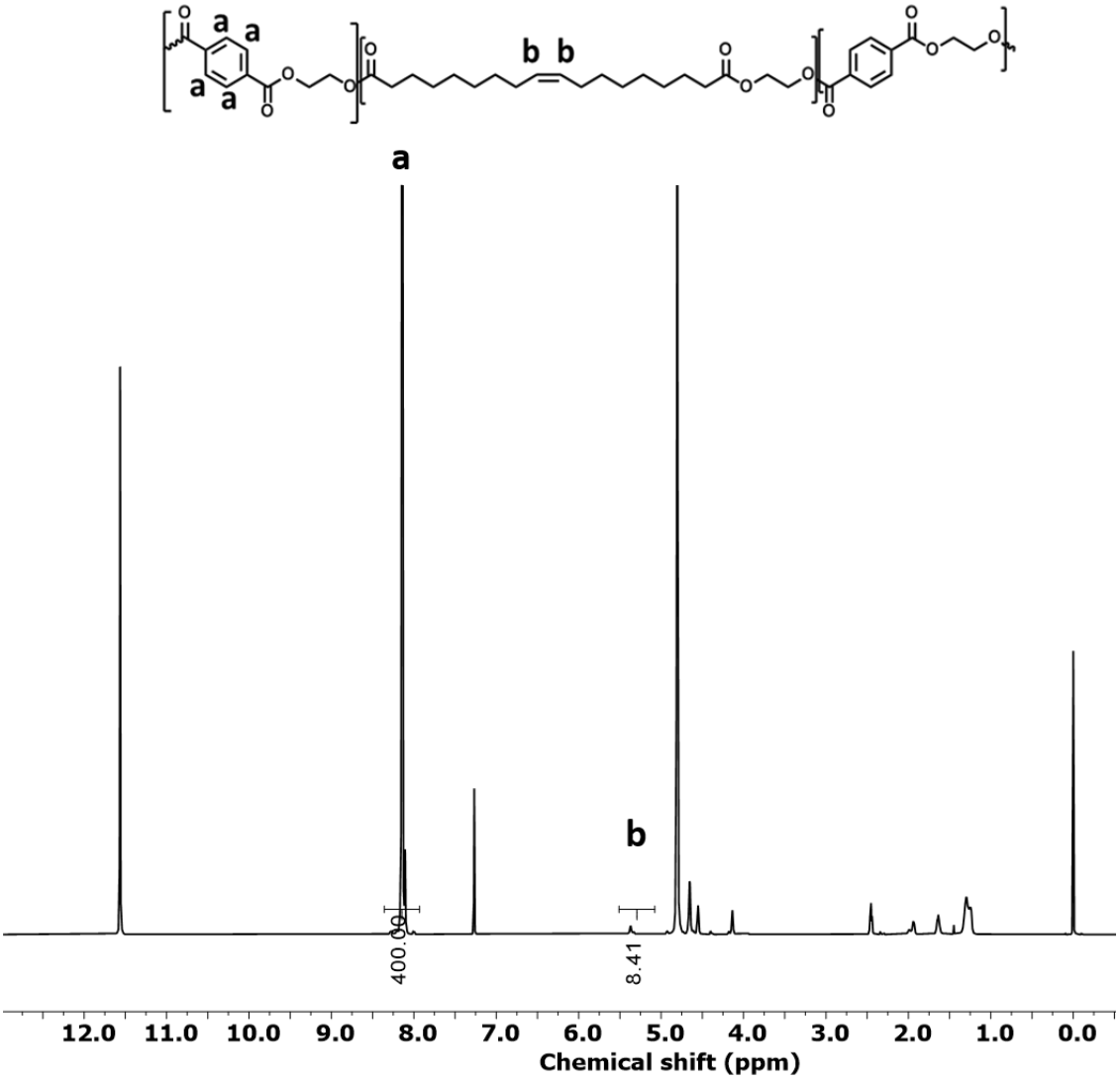

Figure S3 NMR spectra of C18:1-PET copolymer. Peak a shows the aromatic peak, while peak b represents the double bond (sp^2 carbon).

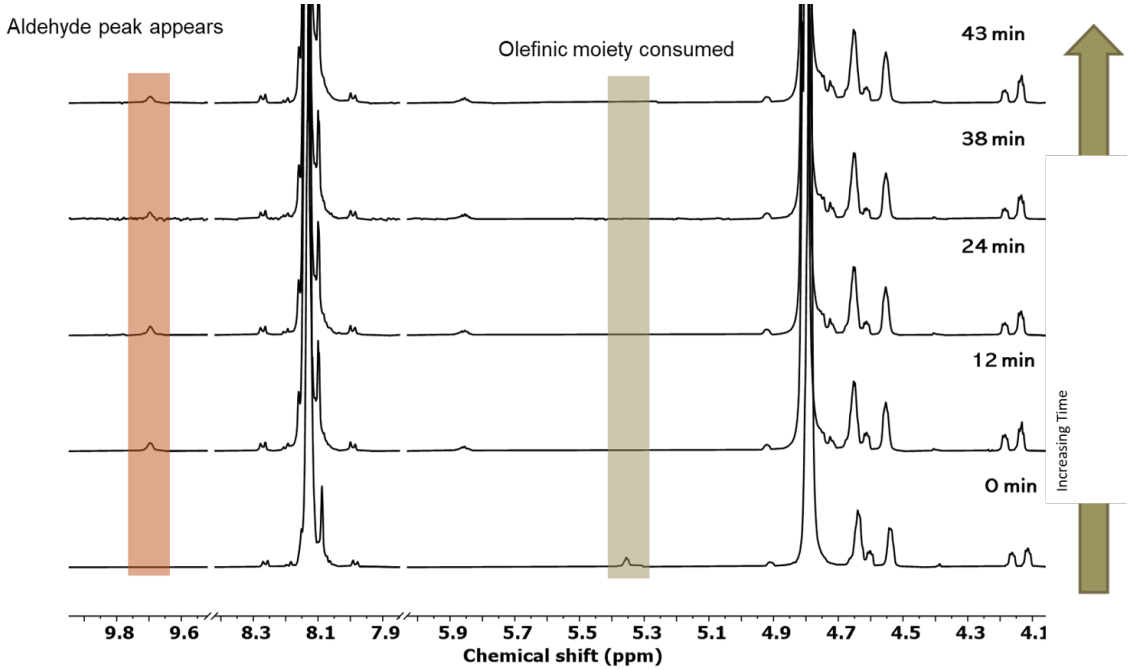

Figure S4 NMR spectra of C18:1-PET copolymer. Peak a shows the aromatic peak, while peak b represents the double bond (sp^2 carbon). The ozonolysis is conceivably completed before 12 mins as the later time stamps show no presence of olefinic moiety.

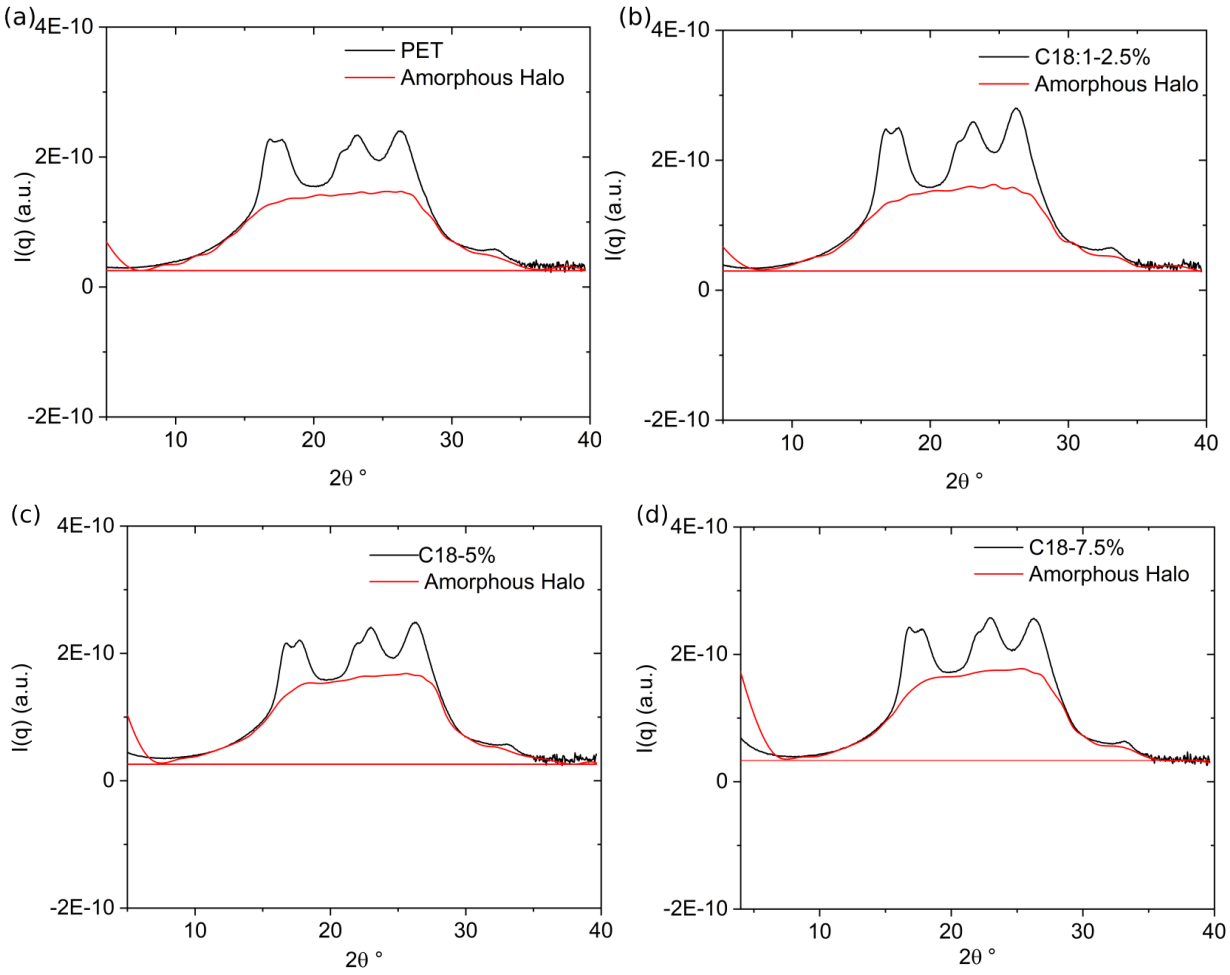

Figure S5 (**a**) Lab-PET WAXS diffraction pattern. Injection-molded PET samples annealed at 150°C for 24h were analyzed by WAXS. (**b**) WAXS diffraction pattern of 2.5%-C18 formulations annealed at 150°C for 24h (**c**) WAXS diffraction pattern of 5%-C18 formulations annealed at 150°C for 24h (**d**) WAXS diffraction pattern of 7.5%-C18 formulations annealed at 150°C for 24h

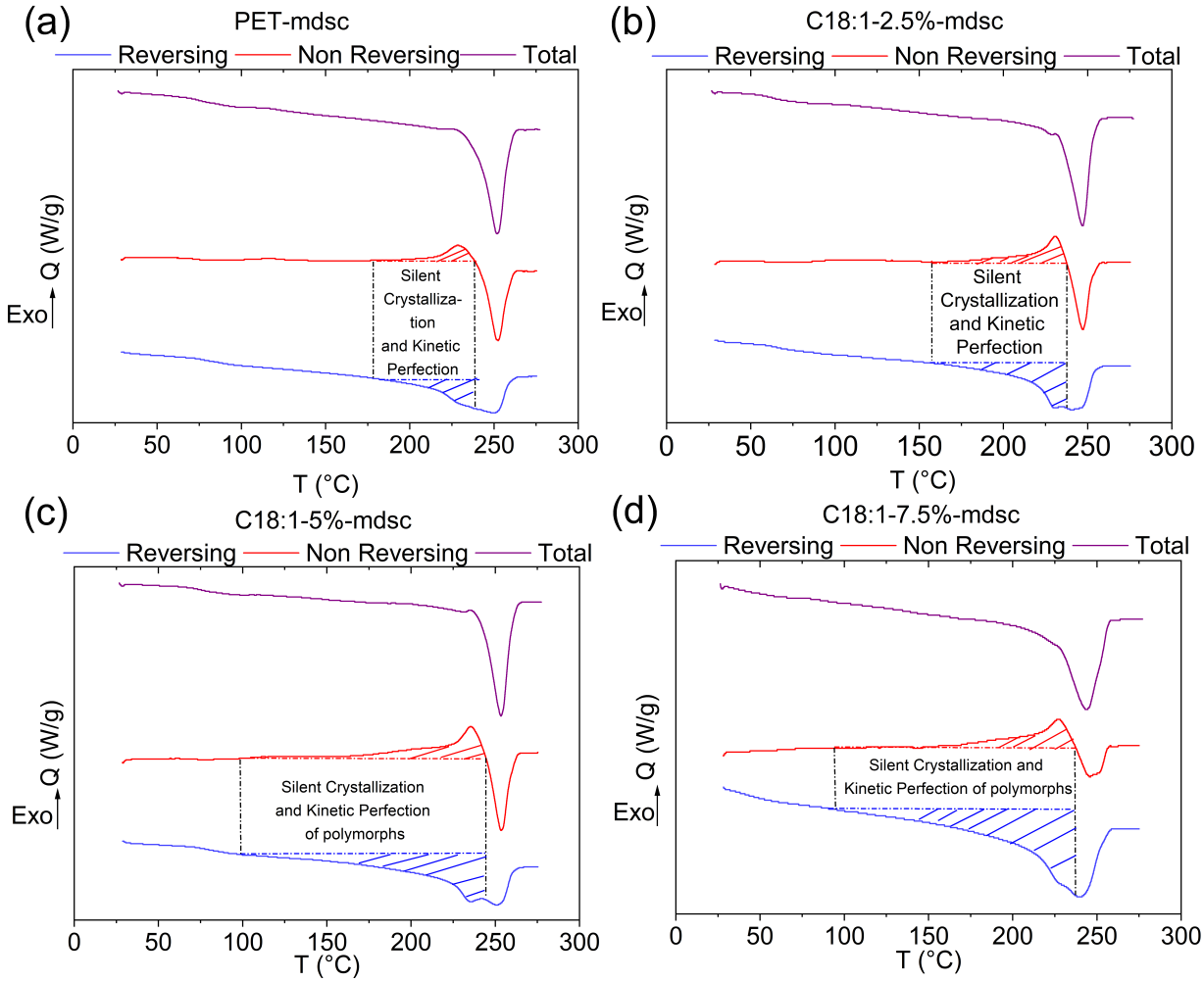

Figure S6 mDSC of C18:1-PET copolymers. **(a)** Lab PET mDSC traces decoupling kinetic and thermodynamic characteristics of melting. **(b)** C18:1-2.5% mDSC traces show a prolonged region for kinetic perfection due to C18 Units. **(c)** C18:1-5% mDSC traces shows a prolonged region for kinetic perfection due to migration of C18 Units. **(d)** C18:1-7.5% mDSC traces illustrate that T_m eventually is also affected along with kinetics of crystallization.

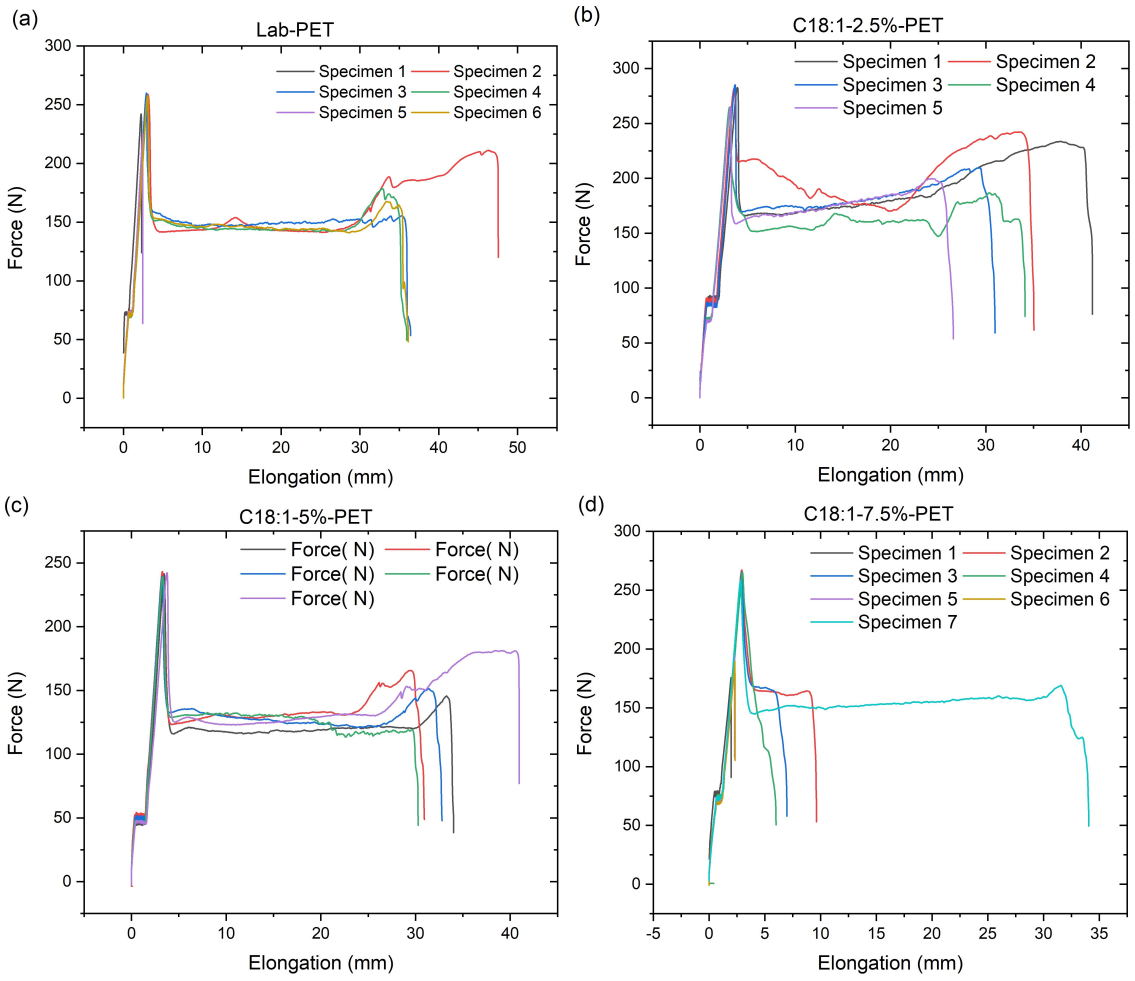

Figure S7 (**a**) Lab-PET tensile characteristics. PET samples follow the regular stress-strain characteristics with strain-induced hardening due to crystallization. (**b**) C18:1-2.5%-PET tensile characteristics. The 2.5% formulation shows a disturbed strain-induced crystallization, most likely due to heterogeneous nucleation sites. (**c**) C18:1-5%-PET tensile characteristics. The 5% formulation marks the reduction in elongation at break characteristics at the prevalent strain rates. (**d**) C18:1-7.5%-PET tensile characteristics. These formulations did not undergo the same elongation at break. This could be due to the defects due to the increased T.H. loadings and the slower crystallization rate, which doesn't lead to strain hardening at 10 mm/min.

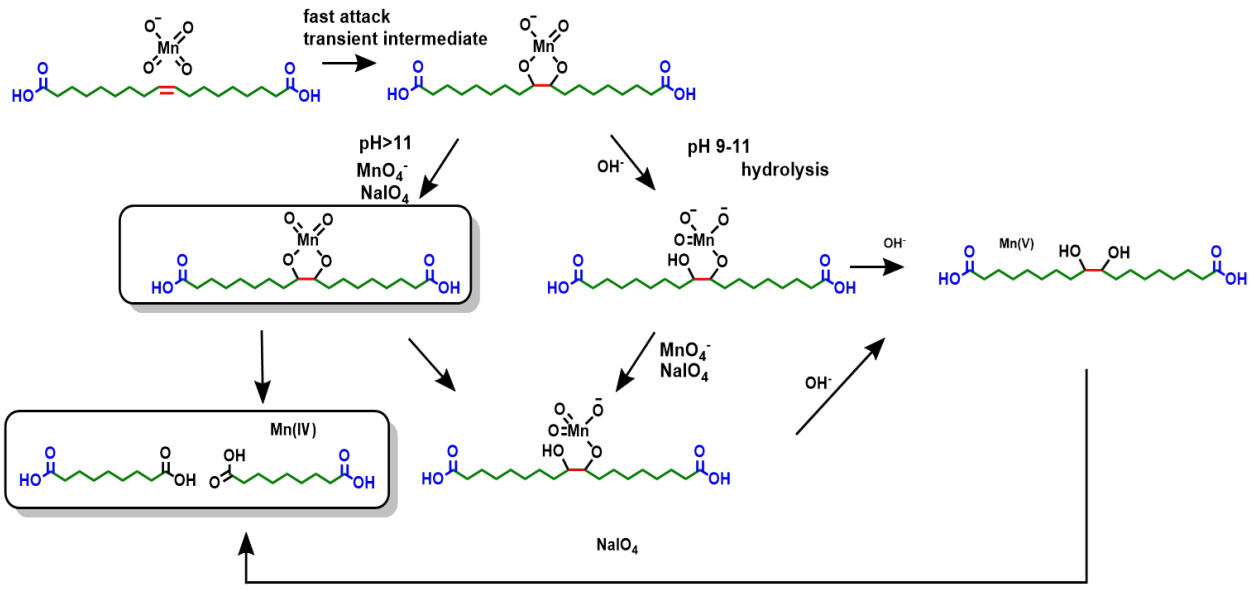

Figure S8 Potential reaction mechanism of potassium permanganate and potassium periodate couple on C18:1 counits. The presence of periodate ensures that the diol is cleaved and the manganate is reoxidized to permanganate, maintaining a stronger oxidative environment.

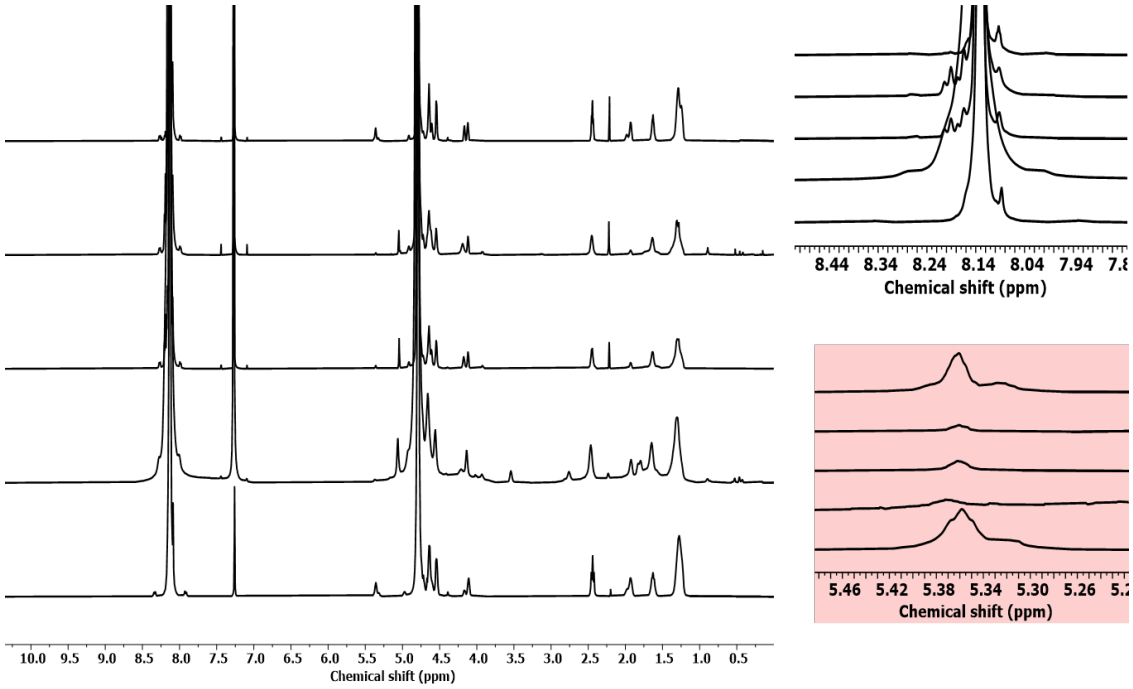

Figure S9 NMR spectra of C18:1-PET pre- and post-permanganate/periodate oxidation. The double bond gets consumed for the C18:1 formulation in the presence of an oxidant. As oligomers form, the terephthalic region (aromatic region) develops ramifications showing bulk depolymerization; however, in the absence of oxidation, primarily surface and end chain hydrolysis prevail.

TOC Graphic

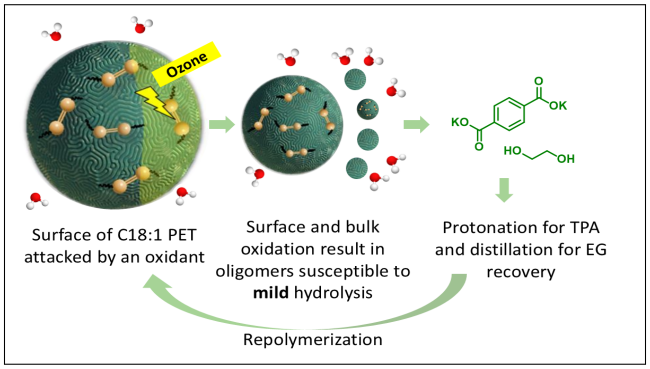

The figure shows two-stage bulk depolymerization of C18:1-PET copolymers undergoing mild oxidative-hydrolysis.